SPEKTRA: Jurnal Fisika dan Aplikasinya
Volume 11, Issue 2, August 2026
Homepage: doi.org/10.21009/SPEKTRA

DOI: doi.org/10.21009/SPEKTRA.112.03

Imaging Performance Analysis of Green Mussel Shell-Derived Hydroxyapatite as a Sustainable Material for Bone Phantom Fabrication

Zhevanya Elisa Cleans Sihombing[1], Devina Rayzy Perwitasari Sutaji Putri[1], Erlinda Ratnasari Putri[1], Adrianus Inu Natalisanto[2], Sahara Hamas Intifadhah[3,*]

[1]*Medical Physics, Department of Physics, Faculty of Science and Mathematics, Mulawarman University, Samarinda 75123, Indonesia*
[2]*Theoretical Physics, Department of Physics, Faculty of Science and Mathematics, Mulawarman University, Samarinda 75123, Indonesia*
[3]*Material Physics, Department of Physics, Faculty of Science and Mathematics, Mulawarman University, Samarinda 75123, Indonesia*

*Corresponding Author Email: saharahamas@fmipa.unmul.ac.id

Received: 23 January 2026
Revised: 6 August 2026
Accepted: 28 August 2026
Online: 30 August 2026
Published: 30 August 2026

SPEKTRA: Jurnal Fisika dan Aplikasinya
p-ISSN: 2541-3384
e-ISSN: 2541-3392

CC BY

ABSTRACT

Bone phantom is a testing tool in radiology used to mimic the radiological properties of human bone tissue, with hydroxyapatite (HA) as one of its key mineral components. In this study, HA was synthesized from green mussel shells (Perna viridis) through two different shell preparation methods, namely HA 1 produced by calcining the shells in whole (uncrushed) form and HA 2 produced by calcining the shells after they had been crushed into powder. The mussel shell powder was first characterized using an Atomic Absorption Spectrophotometer (AAS) to determine its Calcium Oxide (CaO) content, followed by X-Ray Diffraction (XRD) after the HA synthesis process to confirm the formation of the HA material. Each HA powder was mixed with rice bran at ratios of 1:1, 1:2, and 2:1 to fabricate bone phantom prototypes, which were subsequently evaluated through X-Ray Radiography and CT-Scan imaging. Radiographic images were analyzed to obtain the mean gray value, hereafter reported as Optical Density (OD), while CT images were analyzed to obtain Hounsfield Unit (HU) values; both were compared against the reference radiodensity range of human bone. AAS analysis showed that the CaO content of the green mussel shells was 30.89%, and XRD confirmed the presence of HA diffraction peaks in a semi-crystalline phase for both HA 1 and HA 2. The highest OD value, 142.76, was obtained from HA 1 (whole-shell calcination) at a 1:1 ratio and 40 kVp, while the highest HU value, 2180.67 HU, was obtained from HA 2 (crushed-shell calcination) at a 1:1 ratio and 80

kV, a value that falls within the Hounsfield range of cortical bone (+700 to +3000 HU). These results indicate that the 1:1 ratio produced the most bone-equivalent radiodensity for each respective HA type, supporting the potential of green mussel shell-derived hydroxyapatite as a low-cost, sustainable material for bone phantom fabrication. This study contributes a reproducible, low-cost protocol for converting an underutilized marine waste stream into a bone-equivalent phantom material, together with quantitative OD and HU benchmarks across HA-type, composition-ratio, and exposure-voltage combinations, providing an empirical basis for the wider adoption of biogenic hydroxyapatite phantoms in radiological quality assurance and medical physics education.

Keywords: Bone Phantom, Green Mussel Shell, Hydroxyapatite, Hounsfield Unit, Optical Density

INTRODUCTION

Bone is one of the essential organs in the human body that functions as a structural framework supporting body weight, protecting vital organs, providing attachment sites for muscles, and serving as a reservoir for minerals and bone marrow for hematopoiesis [1]. However, bone integrity can deteriorate due to aging, osteoporosis, congenital deformities, trauma, or malignancies, leading to bone defects that require medical intervention or replacement [2]. To address these issues, researchers have focused on developing biomaterials and bone phantoms that can replicate the physical and radiological characteristics of natural bone for medical imaging and diagnostic calibration purposes [3].

A phantom is an artificial human body model used in radiology to simulate tissue properties and evaluate imaging system performance. It allows the testing of imaging parameters and radiation dose without involving patients, thus enhancing safety and accuracy in diagnostic procedures [4]. Phantoms are also used in radiation dosimetry and equipment calibration, ensuring the reliability of imaging systems. An ideal phantom material should possess radiological properties that closely resemble human tissues, particularly in terms of optical density (OD) and Hounsfield Unit (HU) values [5]. The ability of a phantom to mimic bone radiodensity plays a crucial role in achieving consistent and realistic imaging simulations.

Optical Density (OD) traditionally refers to the degree of blackening on a radiographic film, indicating the amount of X-ray absorption through an object [6]. In digital radiography, this film-based OD is commonly approximated by the mean gray value, i.e. pixel intensity on a scale of 0 (black) to 255 (white), extracted from the digital image, where a darker or denser region corresponds to a distinct gray-level response [7]. According to [6], the optimal optical density for bone tissue ranges between 0.25–2.5. OD is therefore a critical factor in evaluating radiographic image contrast and film response. In this study, the term “optical density” refers specifically to the mean gray value extracted from digital radiographs using ImageJ software, without calibration against a physical step-wedge of known density; the reported values therefore represent a relative digital OD surrogate rather than an absolute, calibrated film

optical density. However, OD alone is insufficient to determine material suitability; it should be complemented by CT-based quantitative measurements.

In Computed Tomography (CT), tissue density is represented by Hounsfield Units (HU), a standardized quantitative scale for radiodensity. Air corresponds to −1000 HU, water to 0 HU, and cortical bone typically ranges between +700 and +3000 HU [8]. HU values are directly proportional to the attenuation coefficient of X-rays within tissues, making them highly reliable for differentiating material density [9]. Therefore, the combination of OD and HU analysis offers a comprehensive assessment of how closely a material resembles actual bone in radiological imaging.

One promising natural biomaterial for phantom development is the green mussel (*Perna viridis*) shell, a marine organism abundant along the Indonesian coastline. The shell primarily consists of calcium carbonate ($CaCO_3$) up to 99.5%, along with other minerals such as calcium phosphate, calcium bicarbonate, and calcium sulfide [10]. Upon calcination, these compounds can form calcium oxide (CaO) and hydroxyapatite (HA), the main mineral components of bone [11]. The chemical composition and crystalline structure of HA synthesized from mussel shells have shown significant potential for mimicking the physical and radiological properties of human bone [12]. Utilizing green mussel shells for phantom fabrication not only provides an eco-friendly solution but also adds value to marine waste materials [13]. Hydroxyapatite ($Ca_{10}(PO_4)_6(OH)_2$) is a calcium phosphate bioceramic known for its biocompatibility, bioactivity, and structural similarity to natural bone [14]. It is widely used in orthopedics and dentistry for bone grafts, coatings, and scaffolds. The synthesis of HA from biogenic sources such as seashells, eggshells, and coral has been extensively studied due to their high calcium content and accessibility [15]. The green mussel shell, in particular, offers an excellent calcium source for HA synthesis with a lower environmental impact compared to conventional methods.

Previous studies have investigated the potential of various natural materials in phantom fabrication. For example, [2] developed a phantom from pearl oyster shells mixed with rice bran, yielding OD values close to those of human bone; however, physical imperfections such as air bubbles reduced material homogeneity. [16] utilized local wood as a phantom substitute, but the resulting images lacked optimal radiographic contrast. Other studies, such as those by [17], highlighted the importance of exposure parameters (kVp and mA) in determining OD and HU accuracy. These findings collectively emphasize the need for a more consistent and bone-equivalent material.

Based on these insights, the present study focuses on utilizing green mussel shells (*Perna viridis*) as a raw material for the synthesis of hydroxyapatite-based bone phantoms. The research aims to analyze their optical density (OD) and Hounsfield Unit (HU) values under various composition ratios and exposure voltages. The results are expected to demonstrate the radiological equivalence of mussel shell-derived HA to human bone, offering a low-cost, sustainable alternative for medical imaging calibration and educational applications [18].

Beyond material composition, phantom performance is also influenced by exposure parameters and material homogeneity. Lower tube voltage enhances image contrast through

increased photoelectric interaction, whereas higher voltage increases photon penetration and reduces density differentiation [17]; inhomogeneous material containing air voids or uneven particle distribution can likewise introduce artifacts and inaccurate OD or HU measurements [19]. From a broader perspective, converting green mussel shell waste, abundant yet largely underutilized in Indonesia's aquaculture and seafood industry, into hydroxyapatite-based biomaterials supports sustainable waste management and offers a low-cost alternative to commercial phantom materials [13], with the added benefit of supporting medical physics education and radiological quality assurance in resource-limited settings [16].

METHODS

Material Preparation

This study was carried out through several consecutive steps. The first step was the preparation of green mussel shell powder as shown in FIGURE 1. Green mussel shells were thoroughly cleaned, sun-dried, and heated in an oven at 90°C for 15 minutes to remove residual moisture. Two shell preparation routes were then applied prior to calcination, producing two distinct HA powders, HA 1 and HA 2. For HA 1, the cleaned shells were calcined directly in their whole, uncrushed form. For HA 2, the cleaned shells were first crushed and ground into powder before calcination. Both HA 1 and HA 2 were then calcined at 1000°C for 6 hours, converting calcium carbonate ($CaCO_3$) into calcium oxide (CaO), which serves as a precursor of hydroxyapatite (HA). This phase-change process occurs due to thermal decomposition. The thermal decomposition (calcination) of calcium carbonate is a single-step endothermic reaction described by the following reaction equation:

$$CaCO_3(s) \rightarrow CaO(s) + CO_2(g)$$

The precursor of hydroxyapatite (HA) that was obtained after calcination, for both HA 1 and HA 2, was ground and sieved to obtain a fine powder with a particle size of -100/+200 mesh. To form the hydroxyapatite phase, a hydrothermal mixing process was carried out using materials consisting of CaO powder (from green mussel shells) and ammonium dihydrogen

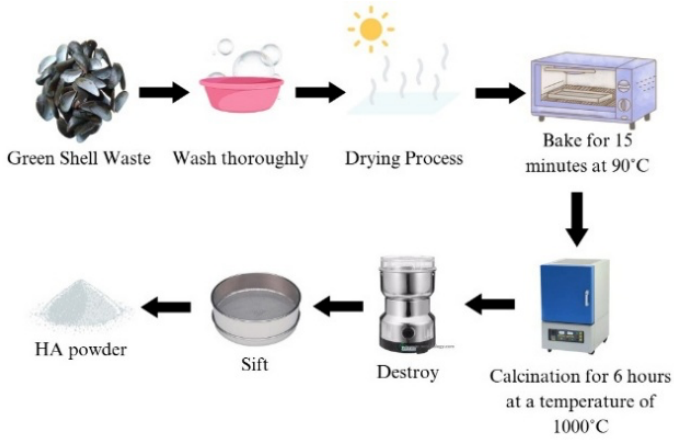

FIGURE 1. Illustration of HA Synthesis Process from Green Mussel Shells

TABLE 1. Summary of HA Shell Preparation Methods and Bone Phantom Sample Variations

Sample	Shell Preparation (before calcination)	$NH_4H_2PO_4$/CaO (gr) + H_2O (600 ml)	HA : Rice Bran Ratio (g)	X-Ray Radiography (kVp)	CT-Scan (kV)
HA 1	Whole shell (uncrushed)	54/46	1:1, 1:2, 2:1	40, 50, 60	80, 100, 120
HA 2	Crushed shell (powder)	54/46	1:1, 1:2, 2:1	40, 50, 60	80, 100, 120

phosphate ($NH_4H_2PO_4$) dissolved in distilled water. A summary of the two shell preparation routes and the resulting phantom sample variations is presented in TABLE 1. The mixing process was carried out at 90°C for 6 hours using a magnetic hotplate stirrer at a stirring speed of 300 rpm. The sample was then dried in an oven for 15 hours until a solid formed. Afterward, calcination was performed at 1000°C for 2 hours to obtain hydroxyapatite (HA) powder. The mechanism of hydroxyapatite phase formation is explained through chemical reactions. These reactions occur in two stages. The first stage is the CaO hydration stage (which occurs rapidly, almost instantly when CaO comes into contact with water), and the second stage is the precipitation/hydrothermal reaction stage.

$$\text{Step 1: } CaO + H_2O \rightarrow Ca(OH)_2$$

$$\text{Step 2: } 10Ca(OH)_2 + 6NH_4H_2PO_4 \rightarrow Ca_{10}(PO_4)_6(OH)_2 + 6NH_3 + 18H_2O$$

$$\text{Step 3: } 10CaO + 6NH_4H_2PO_4 \rightarrow Ca_{10}(PO_4)_6(OH)_2 + 6NH_3 + 8H_2O$$

The next step involved bone phantom fabrication. HA powder was mixed with rice bran, resin, and catalyst, then molded into bone phantoms. Rice bran, resin, and catalyst served as the matrix, while HA powder acted as the filler material. The composition of the catalyst and resin was kept constant at 0.2 g and 50 g, respectively. Meanwhile, the composition of rice bran and HA powder was varied, with ratios of 1:1, 1:2, and 2:1 in grams. The mixture was stirred until homogeneous, poured into plastic molds, and dried in an oven to obtain prototype bone phantoms.

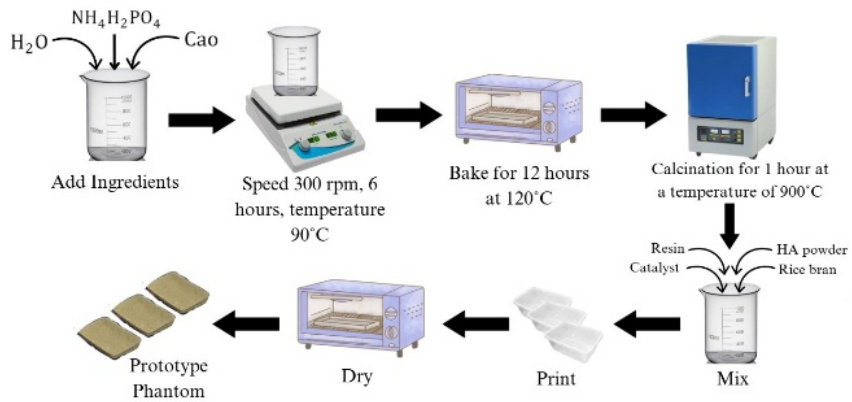

FIGURE 2. Illustration of Bone Phantom Fabrication Process

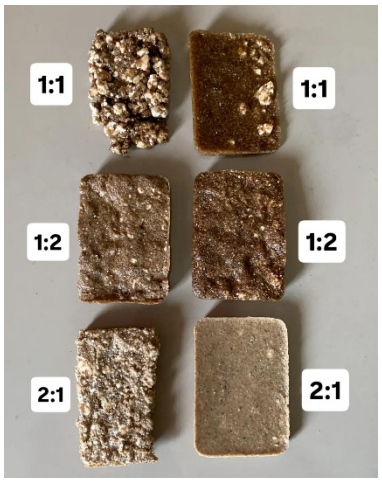

FIGURE 3. Bone Phantom Samples from Green Mussel Shells

The results of the synthesized bone phantom are shown in FIGURE 3. Physically, the bone phantom is brownish in color, with differences based on variations in composition between HA and rice bran. All samples were visually inspected for surface cracking, incomplete binding, and air-void formation prior to imaging, and only visually homogeneous samples were used for radiographic and CT testing; a quantitative porosity or density-uniformity assessment was not performed and is recommended for future studies to more rigorously characterize structural homogeneity across composition ratios.

Material Characterization

The green mussel shell powder was characterized using Atomic Absorption Spectroscopy (AAS), while the HA samples were characterized with X-Ray Diffraction (XRD). AAS is used to determine the chemical composition and XRD is used to confirm the crystalline phase of hydroxyapatite (HA). Furthermore, the bone phantoms were characterized using radiographic testing, namely X-Rays and CT Scans.

AAS is a chemical analysis technique used to determine the concentration of metallic elements by measuring the absorption of light by free atoms. In biomaterial studies, AAS is employed to determine calcium oxide (CaO) content in mussel shells. A high CaO level indicates the potential to exhibit properties similar to bone [10]. After confirming the chemical composition, it is equally important to analyze the crystal structure of the material.

XRD is a non-destructive analytical method that investigates the crystalline structure of materials. By analyzing X-ray diffraction patterns, this technique identifies crystal phases, degree of crystallinity, and particle size. In biomaterial research, XRD is used to verify whether calcined mussel shells successfully form hydroxyapatite [20]. Such structural analysis is critical since crystallinity strongly influences both the mechanical and radiological properties of phantoms. Phase formation was confirmed qualitatively by comparing the diffraction peak positions of the calcined samples with the standard HA reference peak; a quantitative phase-purity determination (e.g., Rietveld refinement) to verify the complete

conversion of CaO to HA was not performed in this study and is recommended for future work.

The next characterization was radiographic testing using X-Rays and CT-Scans. The phantoms were exposed to X-ray imaging at 40, 50, and 60 kVp with 10 mAs, and CT scanning at 80, 100, and 120 kV with 10 mA. The resulting images were processed using ImageJ software to determine Optical Density (OD) and Hounsfield Unit (HU) values.

Finally, data analysis was conducted by comparing the OD and HU values obtained from the prototypes with the reference range of human bone. This comparison was used to assess the feasibility of green mussel shell-based materials as bone phantom candidates.

The methodology of this study was designed to ensure that the developed bone phantom material exhibits radiological and physical characteristics comparable to those of human bone. An experimental approach was adopted, as it allows systematic control of variables, including material composition and imaging parameters. Through this approach, each stage of the research process can be quantitatively evaluated to determine the influence of material variation on optical density and Hounsfield Unit values. Experimental methods are widely applied in phantom studies because they provide measurable and reproducible data for validating radiological equivalence [8], [17].

The initial stage of the methodology focused on the preparation and fabrication of bone phantom materials based on hydroxyapatite synthesized from green mussel shells (*Perna viridis*). This process involved raw material preparation, hydroxyapatite synthesis, and material mixing with specific composition ratios to form phantom samples. Variations in composition were applied to observe changes in material characteristics under X-ray exposure. Sample dimensions, thickness, and homogeneity were carefully controlled to ensure that differences in imaging results reflected the effects of material composition rather than geometric or structural factors [2], [19].

Subsequently, the radiological testing procedures were established to obtain both quantitative and qualitative assessments of phantom performance. X-ray radiography was employed for optical density analysis, while computed tomography (CT) imaging was used to measure Hounsfield Unit values. The selection of these imaging modalities was based on their ability to represent material density differences both visually and numerically. The resulting imaging data were then analyzed and compared with reference values of human bone to evaluate the degree of similarity of the phantom material. This methodological framework enables a comprehensive evaluation of phantom characteristics prior to the final analysis and conclusion of the study [8], [16].

To further enhance the reliability and validity of the experimental results, strict standardization of imaging parameters was implemented throughout the radiological examinations. Key parameters, including tube voltage, tube current, exposure time, and filtration, were maintained consistently for all phantom samples during X-ray radiography. This controlled approach is essential to minimize technical variability and ensure that any observed differences in optical density and Hounsfield Unit values are primarily attributed to variations in material composition rather than inconsistencies in imaging conditions. Such

standardization is widely recognized as a fundamental requirement in phantom-based imaging studies to achieve reproducible and comparable measurements [8].

Following image acquisition, a systematic digital image processing and quantitative analysis procedure was applied. Radiographic images obtained from X-ray examinations were imported into digital image analysis software, where grayscale intensity values corresponding to optical density were extracted. Regions of interest (ROI) were carefully defined at predetermined and equivalent locations within each phantom sample to ensure measurement uniformity. In CT imaging, ROI placement was performed on axial slices within the homogeneous regions of the phantom to obtain mean Hounsfield Unit values while minimizing edge effects and partial volume artifacts. The use of ROI-based quantitative analysis improves measurement accuracy and allows consistent comparison of radiological properties across different samples and imaging modalities [8].

In the subsequent analytical stage, the radiological properties of the fabricated phantom samples were systematically compared with reference data for human bone tissue. This comparative evaluation focused on identifying trends, correlations, and relative differences in optical density and Hounsfield Unit values among the various material compositions. Rather than relying solely on absolute numerical values, the analysis emphasized the degree of similarity between the phantom materials and natural bone under equivalent imaging conditions. This approach provides a more robust assessment of radiological equivalence and supports the identification of the most suitable material composition for bone phantom applications. The outcomes of this analysis serve as a critical foundation for the final interpretation of results and facilitate a smooth transition to the concluding methodological discussion and subsequent result analysis [16].

Data processing and analysis were performed using a structured and systematic approach. For each phantom sample, multiple measurements of Optical Density (OD) and Hounsfield Unit (HU) values were obtained to account for potential variability within the material. The resulting data were then averaged to represent the radiological response of each composition. This approach enhances the robustness of the dataset and allows more reliable comparison between different material variations. The processed data were subsequently organized and prepared for statistical and descriptive analysis, forming a solid basis for the presentation and discussion of results in the following sections.

RESULTS AND DISCUSSIONS

The base material of this research was green mussel shells. It was characterized using Atomic Absorption Spectroscopy (AAS) to determine the Calcium Oxide (CaO) content. The result is shown in TABLE 2.

TABLE 2. AAS Result for Green Mussel Shells Powder

Parameter	Unit	Content	Test Method
Calcium Oxide (CaO)	%	30.89	Atomic Absorption Spectrophotometer

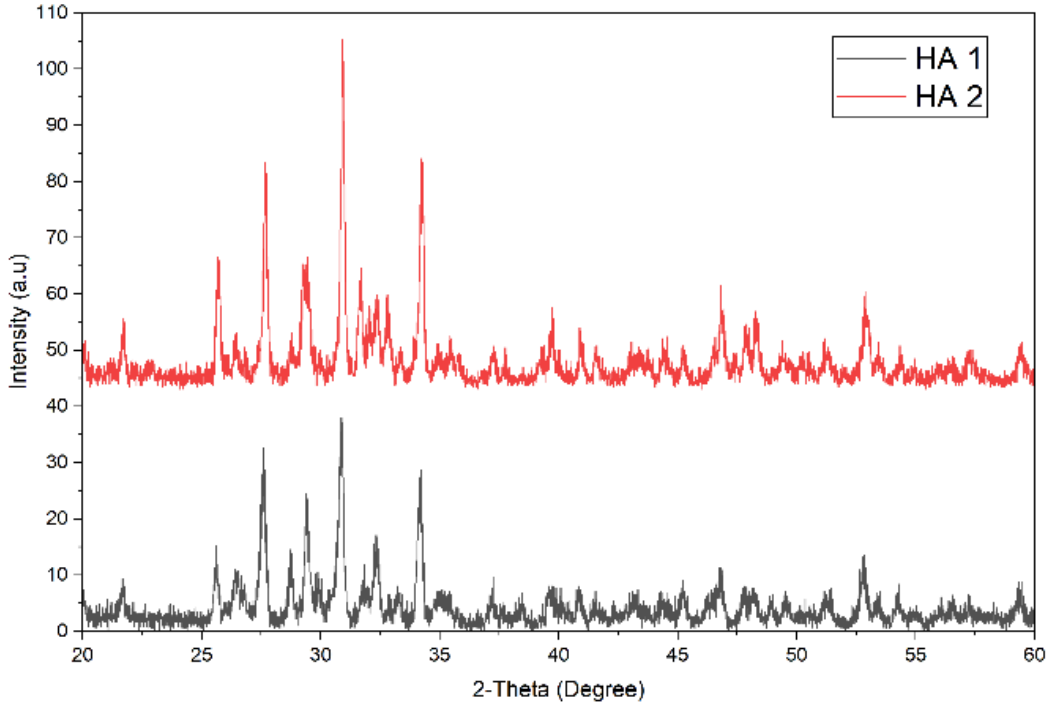

FIGURE 4. XRD Graphs of Hydroxyapatite (HA) Powders, HA 1 (black) and HA 2 (red)

AAS revealed that green mussel shells contain 30.89% CaO, which is close to the calcium content of human bone (±36%) [10]. This high calcium level supports mechanical and crystalline properties, indicating strong potential as a base material for bone phantoms. After processing such as calcination, green mussel shells can serve as an alternative material for radiological research and medical education.

Further characterization was performed to confirm the crystal structure and the formation of the hydroxyapatite (HA) phase, using XRD. Hydroxyapatite (HA) material was obtained from the synthesis of green mussel shells with two different types of treatment. The HA powders consisted of two samples, HA 1 and HA 2. The characteristics of the XRD graph are shown in FIGURE 4.

The X-Ray Diffraction (XRD) showed diffraction peaks within the $2\theta = 30°–32°$ range, consistent with the standard hydroxyapatite (HA) peak (211) at 31.77° [21]. Both HA samples displayed similar diffraction patterns, though they exhibited semi-crystalline properties due to amorphous background interference. This condition is likely caused by the natural origin of green mussel shells and the incomplete calcination process.

The next analysis is radiological testing. Radiological testing was performed on bone phantom samples that had been created previously. The first was using X-Rays radiography to produce images of bone phantoms that are shown in FIGURE 5. The top image is sample HA 1 and the bottom image is HA 2. In this study, the samples consisted of several ratios of HA powder and rice bran, namely 1:1, 1:2, and 2:1 in grams.

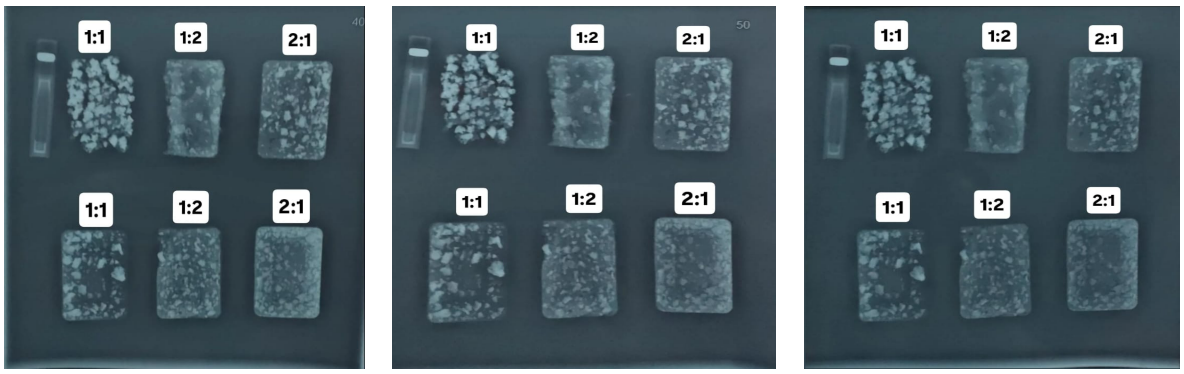

(a) (b) (c)

FIGURE 5. The image of bone phantom from X-Rays radiography using 10 mAs (a) 40 kVp; (b) 50 kVp; (c) 60 kVp

FIGURE 5 shows the radiographic images of the prototype X-ray phantom at voltages of 40, 50, and 60 kVp with a current of 10 mAs. The image at 40 kVp shows the best sharpness and contrast, characterized by clear object boundaries due to the absorption of low-energy X-rays by materials with different densities. At 50 and 60 kVp, the images appear increasingly blurred and the contrast decreases because high-energy X-rays penetrate more without being absorbed, making structural differences less visible. This is in line with the basic principle of radiology that low voltage produces better contrast. In addition, the 1:1, 1:2, and 2:1 material ratios in samples HA 1 and HA 2 also affect image sharpness and contrast based on variations in material density. The result of optical density is shown in TABLE 3.

Bone phantom imaging using X-ray equipment, as presented in TABLE 3 and FIGURE 5, demonstrated significant differences in image contrast across varying tube voltages (40 kVp,

TABLE 3. Optical Density Value Table of Bone Phantom Using X-ray Radiography

Sample	Ratio	Voltage (kVp)	Optical Density
HA 1	1:1	40	142.76
HA 1	1:2	40	111.09
HA 1	2:1	40	120.85
HA 2	1:1	40	112.29
HA 2	1:2	40	91.13
HA 2	2:1	40	113.95
HA 1	1:1	50	127.76
HA 1	1:2	50	109.92
HA 1	2:1	50	113.77
HA 2	1:1	50	111.27
HA 2	1:2	50	105.61
HA 2	2:1	50	126.44
HA 1	1:1	60	126.95
HA 1	1:2	60	107.42
HA 1	2:1	60	102.22
HA 2	1:1	60	105.32
HA 2	1:2	60	98.86
HA 2	2:1	60	112.80

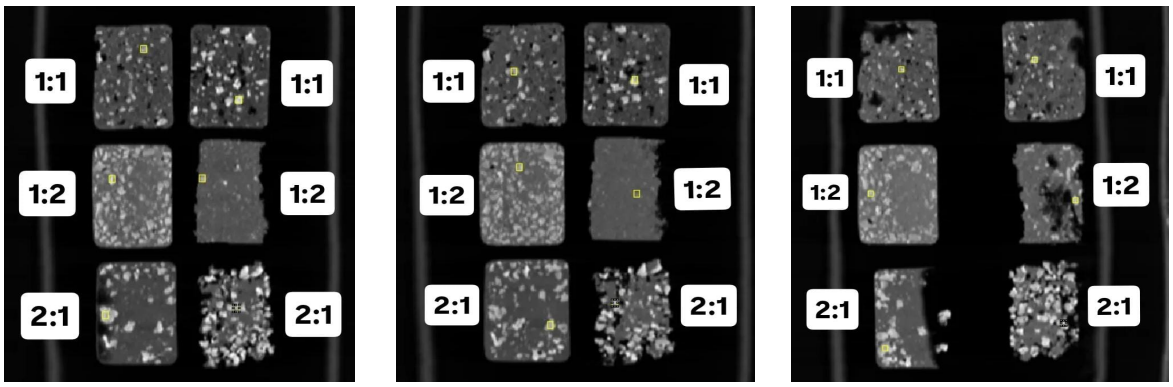

(a) (b) (c)

FIGURE 6. The image of bone phantom from CT-Scan using 10 mA (a) 80 kV; (b) 100 kV; (c) 120 kV

50 kVp, and 60 kVp). At 40 kVp, phantom images appeared sharper, with optical density values closer to that of human bone, particularly in the 1:1 composition, which yielded a value of 142.76. At higher voltages (60 kVp), the images appeared less distinct due to increased photon penetration, reducing density differentiation between materials. Meanwhile, the phantom bone image results using CT-Scan are shown in FIGURE 6.

The results show the prototype phantom images obtained using a CT Scan, where the image on the left is sample HA 1 and the image on the right is sample HA 2. In these samples, ratios of 1:1, 1:2, and 2:1 were used, where the ratio represents a comparison of HA and rice bran. FIGURE 6 shows a prototype bone phantom image using a CT scan with voltage variations of 80 kV, 100 kV, and 120 kV at a constant current of 10 mA, which shows that voltage greatly affects image quality, especially in terms of image sharpness and contrast. A voltage of 80 kV produces the sharpest image with high contrast, while at 100 kV and 120 kV the image quality decreases because the increase in X-ray energy causes deeper penetration without much absorption, resulting in decreased contrast. The images also show six samples with different phantom material ratios (1:1, 1:2, and 2:1), where the 2:1 ratio (more HA) appears brighter due to higher density, while the 1:2 ratio appears darker. This confirms that the material ratio affects image intensity. The result of CT number (HU) is shown in TABLE 4.

Further analysis with CT Scan, as shown in TABLE 4 and FIGURE 6, indicated that the highest Hounsfield Unit (HU) value was obtained from sample HA 2 with a 1:1 ratio at 80 kV, reaching 2180.67 HU. This value falls within the bone category on the Hounsfield scale (+700 to +3000 HU) [8]. Conversely, some compositions produced lower HU values, such as sample HA 2 with a 1:2 ratio at 100 kV, which only reached 463.40 HU, closer to dense soft tissue rather than bone. This suggests that both material ratios and tube voltage significantly influence phantom radiodensity outcomes. In general, the 1:1 and 2:1 ratios at lower voltage (80 kV) most consistently resemble the radiological characteristics of human bone.

In addition to the obtained radiological results, this study is supported by previous research indicating that calcium-based biomaterials, particularly hydroxyapatite, exhibit high radiation attenuation due to their dominant calcium composition. This characteristic makes

TABLE 4. HU Value Table of Phantom Prototype Using CT Scan

Sample	Ratio Composition (gr)	Voltage (kVp)	CT number (HU), Mean ± SD
HA 1	1:1	80	1190.67 ± 421.01
HA 1	1:2	80	1600.31 ± 673.02
HA 1	2:1	80	1911.67 ± 204.40
HA 2	1:1	80	2180.67 ± 394.55
HA 2	1:2	80	1237.17 ± 405.28
HA 2	2:1	80	1500.90 ± 418.72
HA 1	1:1	100	1121.43 ± 373.55
HA 1	1:2	100	1320.80 ± 287.76
HA 1	2:1	100	1668.63 ± 305.38
HA 2	1:1	100	1744.74 ± 490.40
HA 2	1:2	100	463.40 ± 194.35
HA 2	2:1	100	1434.69 ± 408.48
HA 1	1:1	120	866.87 ± 423.12
HA 1	1:2	120	1196.60 ± 204.92
HA 1	2:1	120	1335.37 ± 76.87
HA 2	1:1	120	1273.23 ± 354.25
HA 2	1:2	120	1293.47 ± 351.75
HA 2	2:1	120	1630.27 ± 208.95

hydroxyapatite highly suitable for mimicking human bone tissue in radiological applications [14].

The optical density values obtained in this study tend to decrease with increasing tube voltage (kVp), a trend that is consistent across all sample ratios in TABLE 3. This is in line with radiation interaction theory: as photon energy increases, Compton scattering becomes more dominant over the photoelectric effect, allowing greater photon penetration through the material and reducing the attenuation registered as image density. This finding is also consistent with the qualitative observation in FIGURE 5, where the 40 kVp images exhibited the sharpest contrast while the 60 kVp images appeared progressively less distinct, thus requiring careful optimization of exposure parameters [22].

Furthermore, the Hounsfield Unit (HU) analysis shows that all phantom samples fall within the radiodensity range of human bone (+700 to +3000 HU). This indicates that green mussel shell-based hydroxyapatite has strong potential as an alternative phantom material. Similar findings have been reported in studies utilizing natural calcium sources, which demonstrate comparable density characteristics to human bone [15].

In addition, the microstructure and homogeneity of the material significantly influence radiological outcomes. Non-uniform particle distribution and the presence of microvoids may lead to variations in optical density and HU values. Previous studies have emphasized that particle size and synthesis methods play a crucial role in determining the structural stability and radiological consistency of hydroxyapatite-based materials [23].

This structural consideration also helps explain the HU difference observed between HA 1 and HA 2 in TABLE 4. Although both HA powders exhibited similar diffraction patterns in the semi-crystalline phase (FIGURE 4), the higher HU value obtained from HA 2 (calcined as

crushed shell powder) compared to HA 1 (calcined as whole, uncrushed shell) at the 1:1 ratio and 80 kV (2180.67 HU versus 1190.67 HU) suggests that the pre-calcination particle size may influence the resulting material's radiodensity. Crushing the shells prior to calcination increases the exposed surface area, which likely promotes a more complete and uniform thermal conversion of $CaCO_3$ to CaO throughout the material, whereas whole shells may undergo incomplete or non-uniform conversion in their interior. This difference in conversion completeness and resulting particle packing could plausibly account for the higher HU value observed in HA 2. Quantitative crystallinity analysis, such as Rietveld refinement or crystallite-size estimation, together with a controlled comparison using identical particle sizes prior to calcination, would help confirm whether this radiodensity difference originates primarily from the shell preparation stage or from other processing variables.

CONCLUSION

Based on the results of this study, green mussel shells (*Perna viridis*) have demonstrated strong potential as a raw material for bone phantom fabrication. AAS analysis showed that the calcium oxide (CaO) content of the shells reached 30.89%, relatively close to the calcium composition of human bone, and XRD characterization confirmed the presence of hydroxyapatite (HA) diffraction peaks in a semi-crystalline phase for both HA 1 (calcined as whole, uncrushed shell) and HA 2 (calcined as crushed shell powder), indicating that both shell preparation routes successfully produced a bone-like mineral structure. Radiological evaluation further showed that the highest optical density, 142.76, was obtained from HA 1 at a 1:1 ratio and 40 kVp, while the highest Hounsfield Unit value, 2180.67 HU, was obtained from HA 2 at a 1:1 ratio and 80 kV, a value that falls within the Hounsfield range of cortical bone (+700 to +3000 HU). These findings indicate that, for each respective HA type, the 1:1 HA-to-rice-bran ratio produced the most bone-equivalent radiodensity; however, since HA 1 and HA 2 differed in their pre-calcination shell particle size and were not evaluated under a fully controlled comparative design, the difference in HU response between the two types warrants further investigation, for example through quantitative crystallinity or porosity analysis. Overall, these results support green mussel shell-derived hydroxyapatite as a promising, low-cost, and sustainable candidate material for bone phantom fabrication, while highlighting the need for calibrated optical density measurement against a physical step-wedge and a more systematic comparison between shell preparation methods in future work.

ACKNOWLEDGEMENTS

Z.E.C. Sihombing, D.R.P.S. Putri and S.H. Intifadhah are the main contributors. E.R. Putri and A.I. Natalisanto contributed to the improvement of research methods. All authors read and approved the final version of the paper.

REFERENCES

[1] B. Clarke, "Normal bone anatomy and physiology," *Clin. J. Am. Soc. Nephrol.*, vol. 3, no. suppl. 3, pp. S131–S139, 2008, doi: 10.2215/CJN.04151206.

[2] C. P. Putri Irawan, D. R. P. S. Putri, R. Munir, and Z. Sihotang, "Development of hydroxyapatite-based bone phantoms from blood cockle shells: Effect of material composition on X-ray

attenuation," *J. Penelit. Fis. dan Apl. (JPFA)*, vol. 15, no. 2, pp. 175–186, 2025, doi: 10.26740/jpfa.v15n2.p175-186.
[3] A. W. Sari, A. Olivia Hidayati, D. Mahdo Hapiza, and A. Ridwan, "Pembuatan phantom radiologi menggunakan cangkang kerang sebagai pengganti bahan tulang," *J. Online Phys.*, vol. 8, no. 2, pp. 50–55, 2023, doi: 10.22437/jop.v8i2.22303.
[4] N. Dukov, V.-M. Valkova, M. Yordanova, V. Tsapaki, and K. Bliznakova, "Design and use of a custom phantom for regular tests of radiography apparatus: A feasibility study," *J. Imag.*, vol. 10, no. 10, Art. no. 258, 2024, doi: 10.3390/jimaging10100258.
[5] D. K. Jeong *et al.*, "Effects of energy level, reconstruction kernel, and tube rotation time on Hounsfield units of hydroxyapatite in virtual monochromatic images obtained with dual-energy CT," *Imag. Sci. Dent.*, vol. 49, no. 4, pp. 273–279, 2019, doi: 10.5624/isd.2019.49.4.273.
[6] S. C. Bushong, *Radiologic Science for Technologists: Physics, Biology, and Protection*, 12th ed. Amsterdam, Netherlands: Elsevier, 2020.
[7] C. A. Schneider, W. S. Rasband, and K. W. Eliceiri, "NIH Image to ImageJ: 25 years of image analysis," *Nat. Methods*, vol. 9, no. 7, pp. 671–675, 2012, doi: 10.1038/nmeth.2089.
[8] T. Razi, P. Emamverdizadeh, N. Nilavar, and S. Razi, "Comparison of the Hounsfield unit in CT scan with the gray level in cone-beam CT," *J. Dent. Res. Dent. Clin. Dent. Prospects*, vol. 13, no. 3, pp. 177–182, Oct. 2019, doi: 10.15171/joddd.2019.028.
[9] R. Gautreau and W. Savin, *Modern Physics and Radiation Interaction*. Boston, MA, USA: Addison-Wesley, 2006.
[10] A. Prihanto, S. Muryanto, A. Sancho Vaquer, W. W. Schmahl, R. Ismail, J. Jamari, and A. P. Bayuseno, "In-depth knowledge of the low-temperature hydrothermal synthesis of nanocrystalline hydroxyapatite from waste green mussel shell (*Perna viridis*)," *Environ. Technol.*, vol. 45, no. 12, pp. 2375–2387, 2024, doi: 10.1080/09593330.2023.2173087.
[11] S. Patil, S. Thanikodi, S. Palaniyappan, J. Giri, A. O. Hourani, and M. Azizi, "Sustainable synthesis of marine-derived hydroxyapatite for biomedical applications: A systematic review on extraction methods and bioactivity," *Adv. Manuf.: Polym. Compos. Sci.*, vol. 11, no. 1, Art. no. 2508547, 2025, doi: 10.1080/20550340.2025.2508547.
[12] R. Ismail, T. Cionita, Y. L. Lai, D. F. Fitriyana, J. P. Siregar, A. P. Bayuseno, F. W. Nugraha, R. C. Muhamadin, A. P. Irawan, and A. E. Hadi, "Characterization of PLA/PCL/green mussel shells hydroxyapatite (HA) biocomposites prepared by chemical blending methods," *Materials*, vol. 15, no. 23, Art. no. 8641, 2022, doi: 10.3390/ma15238641.
[13] J. S. R. de Andrade *et al.*, "Sustainable valorization of mussel shell waste: Processing for calcium carbonate recovery and hydroxyapatite production," *J. Funct. Biomater.*, vol. 17, no. 1, Art. no. 24, 2026, doi: 10.3390/jfb17010024.
[14] S. V. Dorozhkin, "Bioceramics of calcium orthophosphates," *Biomaterials*, vol. 31, no. 7, pp. 1465–1485, 2010, doi: 10.1016/j.biomaterials.2009.11.050.
[15] A. Yelten-Yilmaz and S. Yilmaz, "Wet chemical precipitation synthesis of hydroxyapatite from natural sources," *Ceram. Int.*, vol. 44, no. 8, pp. 9703–9710, 2018, doi: 10.1016/j.ceramint.2018.02.201.
[16] W. Mufida, A. P. Utami, and S. N. Dewi, "Pembuatan phantom radiologi berbahan dasar kayu lokal sebagai pengganti tulang manusia," *J. Imejing Diagnostik (JImeD)*, vol. 6, no. 1, pp. 7–10, 2020, doi: 10.31983/jimed.v6i1.5404.
[17] A. A. Oglat, "Comparison of X-ray films in term of kVp, mA, exposure time and distance using Radiographic Chest Phantom as a radiation quality," *J. Radiat. Res. Appl. Sci.*, vol. 15, no. 4, Art. no. 100479, 2022, doi: 10.1016/j.jrras.2022.100479.
[18] M. A. Farrukh, *Principles of Atomic Absorption Spectrophotometry in Material Science*. London, U.K.: Academic Press, 2024.
[19] C. Anam, R. Amilia, A. Naufal, A. T. Maya, and Y. Dwihapsari, "The CT number uniformity and homogeneity: Which is better for detecting the beam hardening artefacts?," *J. Teknol.*, vol. 87, no. 2, pp. 253–261, 2025, doi: 10.11113/jurnalteknologi.v87.21985.

[20] Z. Zuliantoni, W. Suprapto, P. H. Setyarini, and F. Gapsari, "Extraction and characterization of snail shell waste hydroxyapatite," *Results Eng.*, vol. 14, Art. no. 100390, 2022, doi: 10.1016/j.rineng.2022.100390.
[21] A. R. Noviyanti, I. Rahayu, R. P. Fauzia, and Risdiana, "The effect of Mg concentration to mechanical strength of hydroxyapatite derived from eggshell," *Arab. J. Chem.*, vol. 14, no. 4, Art. no. 103032, 2021, doi: 10.1016/j.arabjc.2021.103032.
[22] J. T. Bushberg, J. A. Seibert, E. M. Leidholdt, and J. M. Boone, *The Essential Physics of Medical Imaging*, 3rd ed. Philadelphia, PA, USA: Lippincott Williams & Wilkins, 2012.
[23] J. C. Elliott, *Structure and Chemistry of the Apatites and Other Calcium Orthophosphates*. Amsterdam, Netherlands: Elsevier, 1994.